electronics

MDPI

Article

Multiantenna-Cognitive-Radio-Based Blind Spectrum Sensing under Correlated Signals and Unequal Signal and Noise Powers

Lucas dos Santos Costa, Fátima Sayury Queralt Queda Alves and Rausley Adriano Amaral de Souza *

National Institute of Telecommunications (Inatel), Santa Rita do Sapucaí 37540-000, Brazil; lucass@inatel.br (L.d.S.C.); fatimasayury@get.inatel.br (F.S.Q.Q.A.)
* Correspondence: rausley@inatel.br

Abstract: Adopting cognitive radios (CRs) having multiple antennas in blind non-cooperative and cooperative spectrum sensing (CSS) under fading channels has gained attention due to higher detection performances provided by the spatial diversity gain of multi-sensors in different geographical locations and lower complexity, respectively. However, most studies do not consider sensing scenarios of more practical significance: for example, sometimes adopting only uncalibrated antenna arrays and sometimes only correlated signals at antenna arrays of CRs, but almost always, none of these impairments. Therefore, this paper studies these combined impairments on the performances of two blind techniques in centralized CSS with decision fusion (DF) and data fusion for different numbers of CRs and antennas per CR, both under frequency selective fading channels. One is the circular folding cooperative power spectral density split cancellation (CFCPSC), and the other is the generalized likelihood ratio test (GLRT). Extensive numerical results show, for instance, that with sample fusion (SF) and calibrated antennas, GLRT outperforms CFCPSC independently of correlation, numbers of antennas, or CRs. However, uncalibrated antennas severely penalize GLRT while surprisingly benefiting CFCPSC. Correlation is detrimental to GLRT and CFCPSC with SF but may help CFCPSC in DF and GLRT in DF or eigenvalue fusion. Generally, CFCPSC outperforms GLRT.

Keywords: centralized cooperative spectrum sensing; multiantenna sensor; correlation; uncalibrated antennas; GLRT; CFCPSC; decision fusion; data fusion

Citation: dos Santos Costa, L.; Alves, F.S.Q.Q.; de Souza, R.A.A. Multiantenna-Cognitive-Radio-Based Blind Spectrum Sensing under Correlated Signals and Unequal Signal and Noise Powers. *Electronics* **2022**, *11*, 1719. https://doi.org/10.3390/electronics11111719

Academic Editor: Francisco Falcone

Received: 22 April 2022
Accepted: 23 May 2022
Published: 28 May 2022

1. Introduction

The unprecedented offer for the current explosive amount of new telecommunication services is among many benefits of the evolution of communication systems in the last decades. The improvements provided from older generations of mobile communication systems to its fifth generation (5G) and the advent of the Internet of things (IoT) [1], for instance, have allowed a significant increase in the users quality of service (QoS) and quality of experience (QoE) also driving the traditional concept of wireless communication to a new age in which everyone can connect to everything, everywhere, and at any instant [2]. Moreover, as wireless technologies are continuously under enhancement [3] and evolutions occur pretty fast, lots of new features, applicabilities, and solved problems become available all the time. Indeed, 5G and IoT were just born a few years ago, but even so, several academic research projects and companies are already researching the sixth generation (6G) of mobile communication systems around the world [4]. The above statements and statements in [3] indicate that the introduction of new technologies may occur soon, yet with the potential to revolutionize the existing ones. However, a drawback of the rapid evolution of communication systems is the lack of spectrum bands available to allocate such a large amount of new telecommunication services. That lack of spectrum resources is usually called spectrum scarceness.

Spectrum scarceness can be understood as the result of the growth in demand for additional spectrum bands in the last decades. On the other hand, studies on literature

show that although scarce, spectrum resources are also contradictorily underused [5]. According to these studies, the main reasons for spectrum underutilization are both (i) the procedure regarding the spectrum access that, in fact, gives access rights only to primary users for the contracted time-space domains, and (ii) the low utilization of these incumbents in accessing their spectrum bands in the contracted time-space domains. Consequently, regulatory agencies of spectrum access started considering a new spectrum access policy aiming at mitigating underutilization. In this new access policy, primary spectrum bands could opportunistically be used by non-incumbents or secondary users (SUs) if they find idle/vacant primary user (PU) bands. For that reason, the SUs have to be smart devices in order to find and use possibly vacant PU bands without causing harmful interference to PUs. Fortunately, the concept of spectrum sensing based on cognitive radios (CRs) has emerged as a promising solution to this problem since it is the act of sensing the spectrum seeking idle portions for opportunistic use. Thus, in the context of CR-based spectrum sensing, CRs are intelligent SUs capable of providing secondary access to vacant PU bands without causing harmful interference to PUs via spectrum sensing and then mitigating spectrum underutilization and scarceness.

Spectrum sensing (SS) can be carried out by one CR, or SU, in non-cooperative spectrum sensing (nCSS) or by a group of collaborative SUs in cooperative spectrum sensing (CSS). CSS, however, is wider used due to more statistical power in detecting PU signals. One of the main advantages that give more detection performance to CSS is the spatial diversity of SUs in different geographical locations for sensing the spectrum. The spatial diversity in the positions of cooperating SUs allows the secondary network to overcome issues that nCSS generally cannot, like multipath fading, shadowing, hidden PU terminal problems, or a combination of these phenomena [6]. Additionally, CSS may be centralized, distributed, or relay-assisted [6]. In centralized CSS, SUs sense a target PU band and share some sensing information with a central node called fusion center (FC) via a control channel (CC) for making an occupation decision on its occupation state. This kind of information determines two possible fusion rules. The first one, the soft decision fusion rule, also know as data fusion, and the the second, the hard decision (HD) fusion rule, also known as decision fusion (DF). In the soft decision, this sensing information may be the sensing samples that were collected from the received signal after a specified sensing period or a quantity calculated from these samples. The former soft decision is called sample fusion (SF). The latter soft decision mode commonly adopts quantities as energy values [6], eigenvalues of the sample covariance matrix (SCM) of the received signals [6], or power spectral densities (PSDs) [7], for example. In the HD, however, each SU senses the targeted PU band and autonomously takes and sends their individual decisions on the occupation state of the sensed band to the FC.

Whether in SUs or FC, the secondary network of cooperating SUs needs to apply a statistical test to make occupation decisions. SUs or FC fully computes the adopted statistic in HD or soft decision with SF, respectively, but SUs may also partially compute the adopted statistic in soft decision when SF is not in use and leave the remaining computations to the FC. The FC associates all received information to achieve the global collaborative occupation decision in both cases, soft decision or HD. In HD, it combines all received occupation decisions sent by each SU via the K-out-of-U rule [6], where K is the number of decisions favoring the hypothesis that the PU signal is in the band that is sensed, represented by $\mathcal{H}_1$, i.e., the hypothesis that the PU band under sensing is not idle, and U denotes the number of received decisions. In the K-out-of-U rule, the FC takes a final occupation decision favoring $\mathcal{H}_1$ if a minimum of K out of the U received decisions are also in favor of the hypothesis $\mathcal{H}_1$. It decides in favor of $\mathcal{H}_0$ otherwise, in which $\mathcal{H}_0$ represents the hypothesis that the PU signal is absent of sensed band, i.e., the hypothesis that the PU band under sensing is idle. With $K = U$, $K = 1$, or $K = \lfloor U/2 + 1 \rfloor$, the K-out-of-U rule becomes one of its well-known three particular cases named AND, OR, and majority (MAJ) voting rule, respectively, where $\lfloor \cdot \rfloor$ represents the floor function.

1.1. Related Works

There are several statistical tests analyzed in nCSS and CSS in different circumstances and scenarios, and the literature usually classifies them into three categories: non-blind, semi-blind, or blind statistical tests [8–10]. The most known non-blinds are the matched-filter detection and the cyclostationary feature detection. They are classified as non-blind because they need some a priori information regarding the sensing channels formed between the PU transmitter and SUs receivers and/or the PU signal to be detected to compute their statistics. On the other hand, semi-blind statistical tests as the well-known energy detection (ED) and the eigenvalue-based maximum eigenvalue detection [6], also known as Roy's largest root test, are those statistical tests that do not require any a priori information on the sensing channel or PU signal, but use the additive white Gaussian noise (AWGN) power information in their computations. Although simpler than non-blind tests, semi-blind tests are vulnerable to inaccuracies in the noise power estimation, which is usually called noise uncertainty (NU). Therefore, NU is a significant drawback of semi-blind tests that can limit their application range. Blind tests, however, do not require any a priori information regarding sensing channel, PU signal, or noise power information in their computations. Usually, they do not have a better performance than non-blind or semi-blind tests but have lower computational complexity, which is a relevant advantage of blind tests. Besides, performance analyses of blind statistical tests in spectrum sensing have been gaining increasing attention [9] since the above-mentioned a priori information required for non-blind or semi-blind tests is commonly unknown or difficult to know in practice, especially information regarding the PU signal and/or noise power in scenarios of dynamical noise (DN) (when noise power varies over time). Some examples of blind statistical tests are the eigenvalue-based: (i) maximum-minimum eigenvalue detection (MMED) [6], also known as eigenvalue ratio detection; (ii) the generalized likelihood ratio test (GLRT) [6]; (iii) the PSD-based, cooperative power spectral density split cancellation (CPSC) [7]; and (iv) circular folding cooperative power spectral density split cancellation (CFCPSC) [11]. GLRT (and GLRT-based statistical tests) are by far the most popular of these blind tests, especially in multiantenna-CR-based spectrum sensing, and when neither information on PU signal nor precise noise power-knowledge are available. However, even blind tests as GLRT and MMED may still suffer from performance degradation under unequal noise and/or received signal powers (when received signal and/or noises are assumed to have unequal and/or time-varying variances at the inputs of the receivers of the SUs), which may lead to sensors with unequal average signal-to-noise ratios (SNRs). CFCPSC is an improved version of CPSC with more statistical power than its predecessor algorithm. Both are known because their robustness in scenarios of unequal noise and DN and low computational complexity. Thus, these characteristics make them suitable for the analyses at hand.

Multiantenna-transceivers have been used in CR-based SS [12–15] to increase the statistical power for detecting PU signals. For example, authors in [13] adopted different assumptions on the availability of noise power value to propose two eigenvalue-based statistical tests for multiantenna SU SS using the GLRT paradigm. Proposed methods are called arithmetic to geometric mean (AGM) and signal-subspace eigenvalue (SSE), and results show that semi-blind SSE outperforms ED with no NU, and blind AGM performs better than ED under NU. GLRT and other generalized likelihood ratio-based detectors also outperform the ED under NU in [14] in multiantenna-CR-based spectrum sensing. However, Refs. [13,14] adopt calibrated antennas, meaning that the noise power values at the receiver antennas are identical. Authors of [15,16], on the other hand, provide more practical appeal analyses of GLRT-based tests by assuming that each SU antenna may experience a different noise power level. Additionally, the work in [17] proposes a general multiantenna-based detector for spectrum sensing that outperforms other detectors such as AGM, MMED, GLRT, and GLRT-based detectors under calibrated and uncalibrated antennas with known noise power levels and uncalibrated antennas with unknown noise power levels.

Studies in [15–17] highlight the importance of using multiple antennas in SUs for SS when information on PU signal, sensing channels, and/or noise power values may not be available, but they do not consider correlated received signals at the antenna arrays. It is worth remembering that signal correlation is common in multiantenna receivers, for example, due to the proximity between the antennas. Furthermore, as spatial diversity decreases as the correlation increases, one may expect that it causes performance degradation in a given communication environment.Even so, few works consider correlated received signals in multiantenna-CR-based SS analyses [18]. Additionally, authors in [19] affirm that multiantenna-CR-based SS analyses with correlated received signals and uncalibrated antennas are seldom adopted and statements in [17] lead to the same conclusion.

The work in [20] considers GLRT and CFCPSC in centralized CSS with multiantenna-SUs under frequency-selective (FS) sensing channels, unequal signal and noise powers, where the noise power at the front-end of SUs varies independently over time, and different numbers of SUs and antennas per SU. FS channels follow the IEEE 802.22 standard [21,22] for wireless regional area networks (WRANs), and authors consider GLRT with HD and soft decision fusion and CFCPSC in soft decision with total and partial data fusion. For GLRT, HD fusion adopted the fusion rules AND, OR, and MAJ, and soft decision fusion adopted SF and weighted sample fusion (WSF) and eigenvalue fusion (EF) and weighted eigenvalue fusion (WEF). Results in [20] show that CFCPSC outperforms all except weighted GLRT in soft decision SF under DN. However, one can notice that although this work provides several performance analyses of GLRT and CFCPSC in different circumstances and scenarios, it does not consider received signal correlations at the antenna arrays of SUs. The work in [23], on the other hand, provides performance analyses of GLRT and CFCPSC in multiantenna-SUs in centralized CSS under the same FS sensing channels in [20] with received signal correlations at the antenna arrays but does not consider unequal signal nor noise powers. Yet, the work in [23] only adopts non-weighted GLRT in soft decision SF, HD with the fusion rules AND, OR and MAJ, and CFCPSC in soft decision SF compared to the work in [20], but includes analyses of CFCPSC in HD, which is not included in [20]. The results in [23] show that GLRT outperforms CFCPSC in soft decision under correlated signals without DN, but HD CFCPSC achieves better detection performances than HD GLRT and CFCPSC with soft decision or HD is more robust to FS channels.

Although the aforementioned works are enough to provide a basis for the study of this paper, one can notice that they are far from exhaustive. That is, one can find other studies involving performance analyses of multiantenna SUs for nCSS and CSS under calibrated and uncalibrated antennas, unequal signal powers and/or noise powers, or correlated received signals at the antenna arrays, especially in nCSS. However, very few works adopt combinations of these phenomena, and, to the best of our knowledge, there are no performance analyses of the CFCPSC in multiantenna-CR-based SS combining unequal signal powers and noise powers with correlated received signals at the antenna arrays yet.

1.2. Contributions and Structure of the Paper

This paper is an extension of studies in [20,23]. It extends the analyses of [20,23] by adopting unequal signal and noise powers combined with received signals correlation at the antenna arrays of SUs in centralized CSS under FS sensing channels according to the IEEE 802.22 standard for WRAN [22] for different numbers of SUs and antennas per SU. Analyses of CFCPSC with HD in [23] substitutes the analyses of CFCPSC with partial data fusion in [20]. Since this paper does not adopt CC traffic analysis and CFCPSC with total or partial data fusion, it has identical detection performances under error-free CC, which is the case adopted in this study. This paper also proposes a different approach in terms of DN compared to the one in [20]. Specifically, noise powers in [20] are independently and identically distributed at the front-end of each multiantenna-SU assuming equal noise powers, meaning that the noise powers at the antennas of a given SU are identical, and, therefore, calibrated. In this paper, however, we assume unequal noise power at each antenna of each SU, i.e., we assume that the antennas of given SU may be uncalibrated. The

results show a different picture compared to the results in [20] and consistency compared to [23]. Now, detection performances of GLRT are much more affected than in [20] and drastically degrade under DN powers independently if received signals are correlated or not. CFCPSC, on the other hand, has performance improvements while the performances of GLRT degrades, also independently if received signals are correlated or not. The weighting schemes of [20] for WSF and WEF could not bring any performance improvements and, therefore, should not be used in the adopted scenarios. Results are consistent with those in [23], and as in [23], the existence of correlation among received signals can be detrimental or beneficial to the detection performances of spectrum sensing depending on the test statistic under analysis. GLRT performs better than CFCPSC only in a few cases, and CFCPSC is a better choice in the majority of the performance analyses under the adopted spectrum sensing scenarios.

In summary, the contributions of this paper are

1. The performance analyses of [20] combined with correlated received signals at the antenna array of SUs;
2. The performance analyses of [23] combined with unequal signal and noise powers;
3. The combined performance analyses of [20,23] adopting a new DN model in which the noise power levels at each antenna of each SU may vary, which is called dynamical noise, and also are independent and, possibly, non-identically distributed random variables.

The structure of the rest of the paper is organized as follows. Section 2 presents a background on SS as a binary hypothesis testing the problem and the system model, including the DN model, the GLRT, and CFCPSC algorithms in centralized CSS with SF and DF, and the GLRT weighting schemes for SF and EF. Section 3 presents numerical results and discussions, and Section 4 concludes the paper and gives some directions for further related research.

2. Background and Proposed System Model

The secondary users or fusion center decisions in spectrum sensing are modeled by formulating these decisions as a binary hypotheses test $\mathcal{H}_0$ and $\mathcal{H}_1$, where $\mathcal{H}_0$ and $\mathcal{H}_1$ are the hypotheses that the sensed PU band is vacant or not, respectively. Detection performances of spectrum sensing, or the performances of these decisions, are usually analyzed via the probabilities of false alarm and detection. The probability of false alarm represents the chances of having an occupation decision favoring $\mathcal{H}_1$ when the sensed PU band is in fact under $\mathcal{H}_0$, i.e., $P_{\text{fa}} = \Pr(\mathcal{H}_1|\mathcal{H}_0)$, which is also the probability of the test statistic T exceeds a given decision threshold, here denoted as γ, under $\mathcal{H}_0$, that is $P_{\text{fa}} = \Pr(T > \gamma|\mathcal{H}_0)$. The probability of detection means the chances of having an occupation decision favoring $\mathcal{H}_1$ when the sensed PU band is, in fact, under $\mathcal{H}_1$, i.e., $P_{\text{d}} = \Pr(\mathcal{H}_1|\mathcal{H}_1)$, which is also the probability of having $T > \gamma$ under $\mathcal{H}_1$, that is, $P_{\text{d}} = \Pr(T > \gamma|\mathcal{H}_1)$. These probabilities are combined by using the receiver operating characteristic (ROC) metric, which maps P_{fa} and P_{d} under the variation of γ for a given detector. Another metric is the area under the ROC curve, AUC.

Let us consider the above-mentioned binary hypotheses. Given a PU transmitter using one antenna and a multiantenna SUs containing U SUs with L antennas each, the n-th received signal sample at the l-th antenna of u-th SU, with $n = 1, 2, \ldots, N$, $l = 1, 2, \ldots, L$, and $u = 1, 2, \ldots, U$, can be written as:

$$y_{l,u}(n) = \begin{cases} \eta_{l,u}(n) & ;\mathcal{H}_0 \\ \sum_{z=0}^{Z-1} h_{l,u}(z)s(n-z) + \eta_{l,u}(n) & ;\mathcal{H}_1 \end{cases} \quad (1)$$

for a given sensing instant under hypothesis $\mathcal{H}_0$ or $\mathcal{H}_1$, respectively. Variable $\eta_{l,u}(n)$ in (1), $\eta_{l,u}(n) \sim \mathcal{N}(0, \sigma^2_{l,u})$, represents the n-th complex zero_mean-$\sigma^2_{l,u}$_variance AWGN sample received at the l-th antenna of u-th SU. Notice that the noise variances are possibly different not only among SUs, which is a common situation in practice [20], but also possibly different

at each antenna of the u-th SU, meaning that the antennas of u-th SU are assumed to be uncalibrated and, therefore, expected to cause performance degradation [24]. The n-th binary phase-shift keying (BPSK) PU signal sample is written as $s(n)$ and the operation given by the sum in (1) evaluates the convolution of the PU signal with the impulse response of sensing channel formed between the PU transmitter and the l-th antenna of u-th SU. When Z equals 1, the sensing channels are characterized as slow-flat Rayleigh ones, and when Z is greater than 1, they are slow-frequency-selective Rayleigh ones [11].

2.1. Dynamical Noise Model

Noise distribution significantly affects the detection performances of detectors with multiple antennas because they are generally developed assuming that noises are identically distributed at antenna arrays to minimize complexity [24]. Indeed, most of the works consider identically distributed AWGNs in: (i) at the receiver antennas of SUs in nCSS and CSS under SUs with equal average SNRs and (ii) identically distributed AWGNs at the receiver antennas of u-th SU in CSS under unequal noises (i.e., antennas of u-th SU with equal average SNRs but SUs with unequal average SNRs). For example, Ref. [20] adopts unequal noise powers among SUs but equal noise powers at the antennas of u-th SU. According to (1), Ref. [20] adopts $\eta_{l,u}(n) \sim \mathcal{N}(0, \sigma_u^2)$, meaning that each SU may experience a different noise power, but the antenna array of u-th SU is assumed to be calibrated by a suitable technique [24]. The work in [23], on the other hand, adopts equal noise powers even among SUs, i.e., it adopts $\eta_{l,u}(n) \sim \mathcal{N}(0, \sigma^2)$, meaning that all SUs experience identical noise powers inclusive. Mathematically, one can write the DN model adopted in [20] as $\bar{\sigma}_u^2 \sim \mathcal{U}[(1-\xi)\sigma_u^2, (1+\xi)\sigma_u^2]$, where σ_u^2 is the exact value of noise power at u-th SU, $\bar{\sigma}_u^2$ is the time-varying noise power at u-th SU, possibly varying uniformly in the range $[(1-\xi)\sigma_u^2, (1+\xi)\sigma_u^2]$, and ξ, with $0 \leq \xi \leq 1$, is an DN factor used to determine the level of noise power variation at the front-ends of multiantenna-based SUs, not on the l-th antenna of SUs. In practice, however, calibration errors are unavoidable [19] and lead to different noise powers at the antennas of a given SU. Therefore, our paper gives more practical appeal to the analyses at hand by adopting:

$$\bar{\sigma}_{l,u}^2 \sim \mathcal{U}[(1-\xi)\sigma_{l,u}^2, (1+\xi)\sigma_{l,u}^2], \tag{2}$$

where (2) is a more general DN model compared to the one in [20].

2.2. Correlation Model

This work assumes a scenario where the received samples at the L antennas of u-th SU are possibly correlated and partially follows the correlation model adopted in [23]. Therefore, in order to produce correlation on the received signal samples, consider, at first, the matrix $\mathbf{B}_u \in \mathbb{C}^{L \times Z}$ of uncorrelated slow-FS sensing channel gains that affect the received signals at the L antennas of u-th SU given by:

$$\mathbf{B}_u^{\mathrm{T}} = [\mathbf{b}_{1,u}^{\mathrm{T}}, \mathbf{b}_{2,u}^{\mathrm{T}}, \ldots, \mathbf{b}_{L,u}^{\mathrm{T}}], \tag{3}$$

with $\mathbf{b}_{l,u} \in \mathbb{C}^{1 \times Z}$ being the gains of the time variant impulse response of sensing channels between the l-th antenna of the u-th SU and the PU transmitter with Z-tap and T being the matrix transposition. In (3), the gain vectors $\mathbf{b}_{\jmath,u}^{\mathrm{T}}$ and $\mathbf{b}_{\imath,u}^{\mathrm{T}}$ are uncorrelated for $\imath \neq \jmath$. It is possible to obtain the correlated channel gains matrix $\mathbf{H}_u \in \mathbb{C}^{1 \times Z}$ from (3) by making:

$$\mathbf{H}_u = [\mathbf{h}_{1,u}^{\mathrm{T}}, \mathbf{h}_{2,u}^{\mathrm{T}}, \ldots, \mathbf{h}_{l,u}^{\mathrm{T}}, \cdots \mathbf{h}_{L,u}^{\mathrm{T}}]^{\mathrm{T}} = (\mathbf{B}_u^{\mathrm{T}}\mathbf{Q})^{\mathrm{T}} \in \mathbb{C}^{L \times Z}, \tag{4}$$

where $\mathbf{h}_{l,u} = [h_{l,u}(1), h_{l,u}(2), h_{l,u}(3), \ldots, h_{l,u}(Z)]$. The matrix $\mathbf{Q} \in \mathbb{R}^{L \times L}$ can be written as [25]:

$$\mathbf{Q} = \begin{bmatrix} q_{11} & q_{12} & \cdots & q_{1L-1} & q_{1L} \\ 0 & q_{22} & \cdots & q_{2L-1} & q_{2L} \\ \vdots & & \ddots & & \vdots \\ 0 & 0 & \cdots & q_{L-1L-1} & q_{L-1L} \\ 0 & 0 & \cdots & 0 & q_{LL} \end{bmatrix}. \tag{5}$$

The matrix in (5) can be obtained from a matrix $\mathbf{A}$ [25]:

$$\mathbf{A} = \begin{bmatrix} 1 & \rho & \cdots & \rho^{|2-L|} & \rho^{|1-L|} \\ \rho & 1 & \cdots & \rho^{|3-L|} & \rho^{|2-L|} \\ \vdots & & \ddots & & \vdots \\ \rho^{|L-2|} & \rho^{|L-3|} & \cdots & 1 & \rho \\ \rho^{|L-1|} & \rho^{|L-2|} & \cdots & \rho & 1 \end{bmatrix}, \tag{6}$$

in which $\mathbf{A} = \mathbf{Q}^{\mathrm{T}}\mathbf{Q}$ and ρ, with $0 \leq \rho \leq 1$, is the correlation coefficient that leads to a given correlation between received signals at different antenna pairs of each SU. For $\imath \neq \jmath$, the vectors $\mathbf{h}_{\jmath,u}^{\mathrm{T}}$ and $\mathbf{h}_{\imath,u}^{\mathrm{T}}$ in $\mathbf{H}_u$ are now correlated. The elements of the i-th line and j-th column of $\mathbf{A}$, with $i, j = 1, 2, \ldots, L$, are formulated as:

$$a_{ij} = \rho^{|i-j|}. \tag{7}$$

The a_{ij} parameter denotes the correlation between signals at different antenna pairs of each SU. Clearly, the correlation between received signals at a given antenna pair decreases as $|i - j|$ increases if $0 < \rho < 1$, i.e., received signal samples at farther apart antenna pairs are less correlated than those at closer apart antenna pairs, as expected. Likewise, the element of the i-th line and j-th column of matrix $\mathbf{Q}$ in (5), is:

$$q_{ij} = \begin{cases} \sqrt{a_{ij}}, & i = 1, j = i, \\ a_{ij}/q_{ii}, & i = 1, j \neq i, \\ \sqrt{a_{ij} - \sum_{k=1}^{j-1} q_{kj}^2}, & i > 1, j = i, \\ (a_{ij} - \sum_{k=1}^{j-1} q_{ki}q_{kj})/q_{ii}, & i > 1, j \neq i. \end{cases} \tag{8}$$

The z-th element of channel gain, $h_{l,u}(z)$, that affects the received signal at the l-th antenna of u-th SU in (1) is forming matrix $\mathbf{H}_u$ in Equation (4). Therefore, signal samples received at antenna pairs k and j of u-th SU in (1), given by $y_{k,u}(n)$ and $y_{j,u}(n)$ for $n = 1, 2, \ldots, N$, have a non-zero correlation under hypothesis $\mathcal{H}_1$ if $\rho > 0$. Notice also that the correlation model adopted here does not take into account information as, for instance, operation frequencies, separation distances between antenna pairs, and other information related to the propagation environment, as the angle of arrival of received signals and temporal and frequency dispersion [26]. Moreover, ref. [23] considers only separation distances between antenna pairs. These assumptions make this model simpler and suitable for the analyses in this paper since it allows performance analyses of spectrum sensing under different levels of correlation of received signals at the SUs simply by varying the correlation coefficient ρ.

Figure 1 summarizes the before-described systems for the adopted multiantenna-cognitive-radio-based blind SS assuming correlated signals and unequal signal and noise powers.

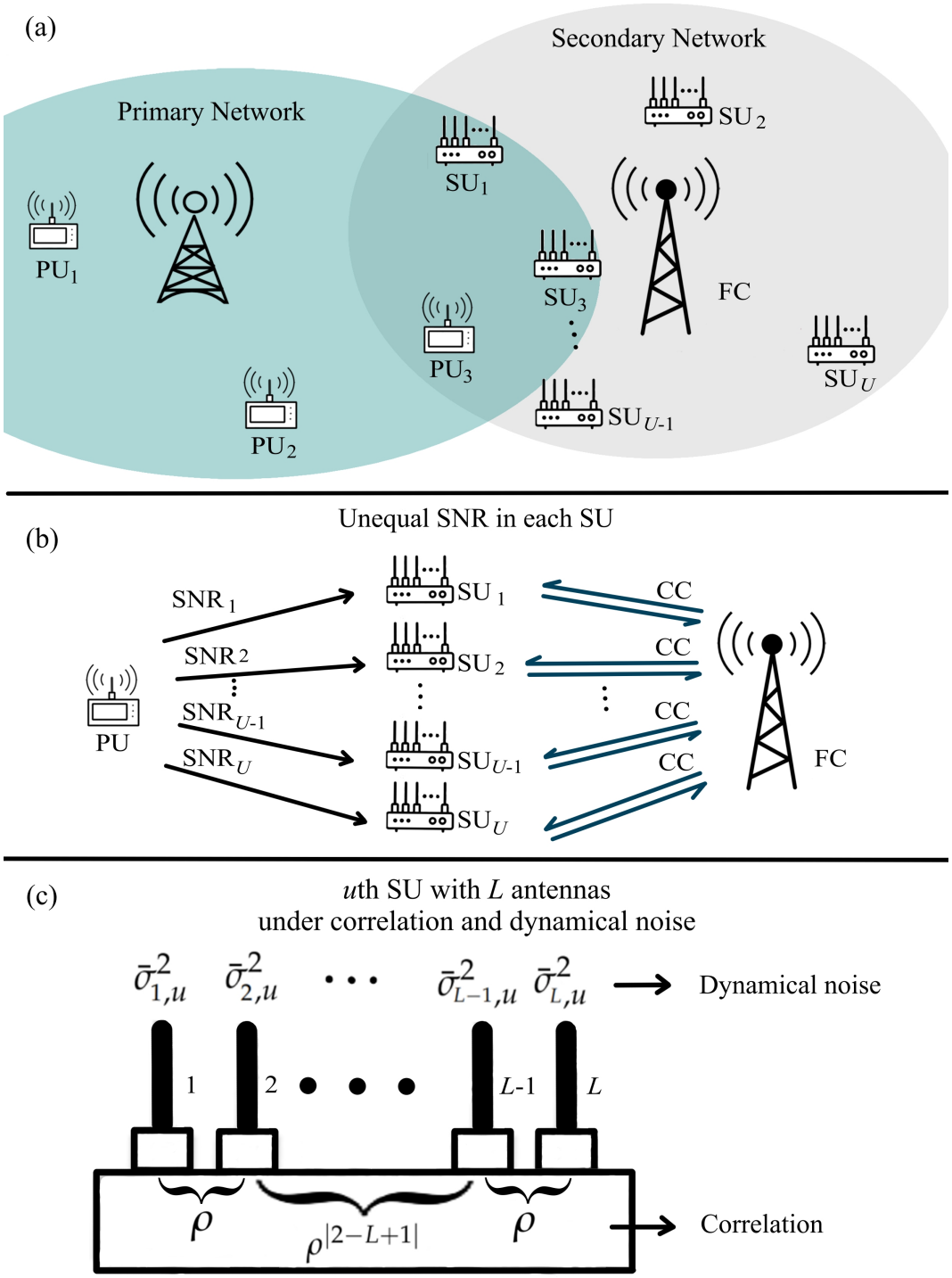

Figure 1. (**a**) Schematic diagram for multiantenna-cognitive-radio-based cooperative spectrum sensing system, (**b**) adopted unequal SNRs, $\{\text{SNR}_1, \text{SNR}_2, \ldots, \text{SNR}_U\}$, among SUs under error-free control channels (CCs), and (**c**) adopted dynamical noise model in which the noise power varies at each antenna of each SU, $\{\bar{\sigma}^2_{1,u}, \bar{\sigma}^2_{2,u}, \ldots, \bar{\sigma}^2_{L,u}\}$, under correlated signals, $\rho^{|i-j|}$ with $i, j = 1, 2, \ldots, L$.

2.3. GLRT

The eigenvalue- and blind-based GLRT [6] is formulated from the SCM of the received signal given by:

$$\mathbf{R} = \frac{\mathbf{Y}\mathbf{Y}^{\dagger}}{N}, \tag{9}$$

where † stands for the conjugate and transpose operation, N denotes the number of samples that was received at each antenna and $\mathbf{Y}$ stands for the received sample matrix.

2.3.1. GLRT with DF

For the GLRT with DF, denoted as GLRT-DF, SUs locally compute the SCM of received signals, its eigenvalues, and the test statistic for making an individual decision on the occupation state of the sensed PU band. SUs send these decisions to the fusion center via the control channels, which combines them for achieving a cooperative decision. It is possible to build the matrix of sensing samples $\mathbf{Y}_u \in \mathbb{C}^{L\times N}$ collected by the L antennas of u-th SU to compute the covariance matrix as:

$$\mathbf{Y}_u^{\mathrm{T}} = [\mathbf{y}_{1,u}^{\mathrm{T}}, \mathbf{y}_{2,u}^{\mathrm{T}}, \ldots, \mathbf{y}_{l,u}^{\mathrm{T}}], \ldots \mathbf{y}_{L,u}^{\mathrm{T}}], \tag{10}$$

where $\mathbf{y}_{l,u} = [y_{l,u}(1), y_{l,u}(2), \ldots, y_{l,u}(N)]$, with $\mathbf{y}_{l,u} \in \mathbb{C}^{1\times N}$, represents the N samples collected by the l-th antenna of u-th SU, and the n-th sample comes from $y_{l,u}(n)$ in (1). Then, the SCM $\mathbf{R}_u \in \mathbb{C}^{L\times L}$ at the u-th SU is:

$$\mathbf{R}_u = \mathbf{Y}_u \mathbf{Y}_u^{\dagger}/N. \tag{11}$$

The u-th SU may compute the GLRT-DF statistic as [6]:

$$T_{\mathrm{GLRT}_u} = \frac{L\lambda_{1,u}}{\sum_{i=1}^{L}\lambda_{i,u}}, \tag{12}$$

such that $\lambda_{1,u} \geq \lambda_{2,u} \geq \cdots \geq \lambda_{L,u}$ are the eigenvalues of $\mathbf{R}_u$ in (11). If $T_{\mathrm{GLRT}_u} > \gamma_u$, the u-th SU makes a decision in favor of hypothesis $\mathcal{H}_1$, or $\mathcal{H}_0$ if $T_{\mathrm{GLRT}_u} > \gamma_u$, where the local decision threshold γ_u is predetermined at u-th SU. The fusion center makes the final decision by applying the K-out-of-U rule, in which the fusion center reaches a final occupation decision favoring $\mathcal{H}_1$ when at least K out of the U sent decisions by the SUs are also in favor of the hypothesis $\mathcal{H}_1$. It decides in favor of $\mathcal{H}_0$ otherwise. When $K = U$, $K = 1$, or $K = \lfloor U/2 + 1 \rfloor$, the K-out-of-U rule becomes AND, OR, MAJ voting rules, respectively, where $\lfloor \cdot \rfloor$ represents the floor function. It is worth highlighting that it is here considered a perfect (error-free) CC, thus occupation decisions sent by SUs and received by the FC are identical.

2.3.2. GLRT with EF and WEF

For the GLRT with EF, denoted as GLRT-EF, the u-th SU also must compute the SCM and its eigenvalues, as it does for the GLRT-DF. Instead of making individual decisions, however, each SU sends its eigenvalues to the FC via CC for final computations and achievement of the cooperative decision on the occupation state of the sensed PU band. The eigenvalues are, therefore, the quantity derived from the received signal samples in this case. Then, in this case, the u-th SU must also compute (11) from (10) and send the eigenvalues of $\mathbf{R}_u$ to the FC. The FC computes the GLRT-EF statistic as [20]:

$$T_{\mathrm{GLRT}_{\mathrm{EF}}} = \frac{L\sum_{u=1}^{U}\lambda_{1,u}}{\sum_{u=1}^{U}\sum_{l=1}^{L}\lambda_{l,u}}, \tag{13}$$

with $\lambda_{1,u} \geq \lambda_{2,u} \geq \cdots \geq \lambda_{L,u}$ being the eigenvalues of u-th SU received at the FC (remembering that the eigenvalues received at the FC are identical to those sent by the SUs since the CC is assumed to be error-free). If $T_{\mathrm{GLRT}_{\mathrm{EF}}} > \gamma_{\mathrm{FC}}$, the FC decides as $\mathcal{H}_1$, or the FC decides as $\mathcal{H}_0$ if $T_{\mathrm{GLRT}_{\mathrm{EF}}} < \gamma_{\mathrm{FC}}$, where γ_{FC} denotes the decision threshold at the FC.

The eigenvalue weighting scheme, denoted as GLRT-WEF, confers robustness to GLRT-EF against the adopted DN model in [20] since it gives more weight to eigenvalues

of SUs affected by lower estimated noise powers. Then it is also used here under the DN model proposed in (2). The weight for the eigenvalues of the u-th SU is given by:

$$g_u = \frac{1}{\hat{\sigma}_u^2} = \left(\frac{1}{L-1} \sum_{l=2}^{L} \lambda_{l,u} \right)^{-1}, \tag{14}$$

where $\hat{\sigma}_u^2 = \frac{1}{L-1} \sum_{l=2}^{L} \lambda_{l,u}$ is the maximum likelihood estimate of the noise power of the u-th SU assuming the presence of a PU signal [6,27]. Notice that $\hat{\sigma}_u^2$ is the mean of the $L-1$ ordered eigenvalues $\lambda_{2,u} \geq \lambda_{3,u} \geq \cdots \geq \lambda_{L,u}$ of the u-th SCM $\mathbf{R}_u \in \mathbb{C}^{L \times L}$ computed in (11). Thus, according to [20], the test statistic for the GLRT-WEF, after some tedious manipulations, can be written as:

$$T_{\text{GLRT}_{\text{WEF}}} = L \left(1 + \frac{U}{\sum_{u=1}^{U} \frac{\lambda_{1,u}}{\sum_{l=2}^{L} \lambda_{l,u}}} \right)^{-1}. \tag{15}$$

2.3.3. GLRT with SF and WSF

For the GLRT with SF, denoted as GLRT-SF, the SUs collect the samples and send them to the fusion center, via CC, reaching a cooperative decision on the occupation state of the sensed PU band. From this point, the FC computes the SCM from the matrix of all received samples $\mathbf{Y}_{\text{FC}} \in \mathbb{C}^{LU \times N}$, its eigenvalues, as well as the test statistic, and makes the decision on the occupation state of the sensed PU band. One can write the matrix $\mathbf{Y}_{\text{FC}}$ according to:

$$\mathbf{Y}_{\text{FC}}^{\text{T}} = [\mathbf{Y}_1^{\text{T}}, \mathbf{Y}_2^{\text{T}}, \mathbf{Y}_3^{\text{T}}, \ldots, \mathbf{Y}_u^{\text{T}}, \ldots, \mathbf{Y}_U^{\text{T}}], \tag{16}$$

with $\mathbf{Y}_u$ being a submatrix of the received signal samples at the FC coming from the u-th SU, which is identical to the u-th matrix in (10) considering an error-free control channel. Then, at the FC, the $LU \times LU$-dimensional complex SCM $\mathbf{R}_{\text{FC}}$ is:

$$\mathbf{R}_{\text{FC}} = \mathbf{Y}_{\text{FC}} \mathbf{Y}_{\text{FC}}^{\dagger} / N, \tag{17}$$

and the FC computes the GLRT-SF statistic as [6]:

$$T_{\text{GLRT}_{\text{SF}}} = \frac{LU\lambda_1}{\sum_{i=1}^{LU} \lambda_i}, \tag{18}$$

with $\lambda_1 \geq \lambda_2 \geq \cdots \geq \lambda_{LU}$ denoting the eigenvalues of $\mathbf{R}_{\text{FC}}$ in (17). The FC makes an occupation decision favoring $\mathcal{H}_1$ when $T_{\text{GLRT}_{\text{SF}}} > \gamma_{\text{FC}}$ or favoring $\mathcal{H}_0$ otherwise, where γ_{FC} is a decision threshold previously established at the FC.

The weighting scheme for received samples, denoted as GLRT-WSF, in [20] confers robustness to GLRT-SF against the adopted DN, then it is also used here under the DN model proposed in (2). Therefore, the matrix of weighted received samples at the FC for the GLRT-WSF can be written as:

$$\mathbf{Y}'_{\text{FC}} = [\mathbf{Y}'^{\text{T}}_1, \mathbf{Y}'^{\text{T}}_2, \ldots, \mathbf{Y}'^{\text{T}}_U]^{\text{T}}, \tag{19}$$

where $\mathbf{Y}'_u = f_u \mathbf{Y}_u$ represents the weighted received samples at the FC related to the u-th SU and f_u is the u-th weight computed according to:

$$f_u = \frac{1}{\hat{\sigma}_u} = \left(\frac{1}{L-1} \sum_{l=2}^{L} \lambda_{l,u} \right)^{-\frac{1}{2}}, \tag{20}$$

where $\hat{\sigma}_u$ is the square root of the maximum likelihood estimate of the noise power of the u-th SU in (14). The FC computes the modified SCM $\mathbf{R'}_{\mathrm{FC}} \in \mathbb{C}^{LU \times LU}$ from the weighted samples in (20) as:

$$\mathbf{R'}_{\mathrm{FC}} = \frac{1}{N} \mathbf{Y'}_{\mathrm{FC}} \mathbf{Y'}^{\dagger}_{\mathrm{FC}}. \tag{21}$$

The GLRT-WSF statistic is calculated as:

$$T_{\mathrm{GLRT_{WSF}}} = \frac{LU\lambda_1^{'}}{\sum_{i=1}^{LU} \lambda_i^{'}}, \tag{22}$$

with $\{\lambda_1^{'}, \lambda_2^{'}, \lambda_2^{'}, \ldots, \lambda_{LU}^{'}\}$ standing for the eigenvalues calculated from (21).

We consider the GLRT-SF as the blind benchmark technique or the state-of-the-art method since it has been largely studied in the last decade.

2.4. CFCPSC

The CFCPSC [11] is a PSD-based blind statistical test known for its robustness against DN and low computational complexity. It was firstly developed for single-antenna SUs in a scenario of centralized CSS with SF. In its computation [23], the algorithm splits the whole bandwidth at each SU into S sub-bands and estimates the power spectral density in each sub-band. Thereafter, it combines the PSD level estimated at the s-th sub-band of all SUs, makes an occupation decision regarding the presence or absence of the PU signal in each sub-band, and finally, combines the sub-band decisions via the OR rule to make a final occupation decision on the sensed PU band. We adopt some modified versions of CFCPSC that work with multiantenna-SUs in SF [20,23] and DF [23]. Sections 2.4.1 and 2.4.2 present these modified versions, respectively.

2.4.1. CFCPSC with SF

For the CFCPSC with SF, denoted as CFCPSC-SF, the CFCPSC algorithm treats each antenna as a separate receiver. This adaptation from the original CFCPSC algorithm [11] is similar to having LU single-antenna SUs instead of U SUs with L antennas each. The corresponding modified algorithm acts in Steps 1 to 5 of the original CFCPSC, leading to the following full algorithm:

1. By using the discrete Fourier transform (DFT), calculate the PSD of the signal at the l-th antenna of u-th SU in (1) as:

$$\mathbf{F}'_{l,u} = \frac{\left|\mathrm{DFT}[y_{l,u}(n)]\right|^2}{N}, \tag{23}$$

   for $n = 1, 2, 3, \ldots, N$.
2. Compute the modified circular-even component of $\mathbf{F}'_{l,u}$ by making:

$$\mathbf{F}_{l,u}(k) = \begin{cases} \frac{[\mathbf{F}'_{l,u}(1) + \mathbf{F}'_{l,u}(N/2+1)]}{2}, & k = 1, \\ \frac{[\mathbf{F}'_{l,u}(k) + \mathbf{F}'_{l,u}(N-k+2)]}{2}, & k = 2, 3, \ldots, N. \end{cases} \tag{24}$$

3. Split the sensed band into S sub-bands and compute the signal power in the s-th sub-band, with $s = 1, 2, \ldots, S$, as:

$$F_{s_{l,u}} = \sum_{k=1}^{N/(2S)} \mathbf{F}_{l,u}[k + (s-1)V]. \tag{25}$$

4. Calculate the total amount of signal power in the band that is sensed as:

$$F_{\text{full}_{l,u}} = \sum_{k=1}^{\frac{N}{2}} \mathbf{F}_{l,u}(k). \tag{26}$$

5. Find the average of the ratios $F_{s_{l,u}} / F_{\text{full}_{l,u}}$ in order to eliminate the effect of the noise variance, leading to:

$$r_{u,s} = \sum_{l=1}^{L} \frac{F_{s_{l,u}}}{L F_{\text{full}_{l,u}}}. \tag{27}$$

6. At the FC, compute the test statistic for the s-th sub-band as:

$$T_{\text{CFCPSC}_s} = \frac{1}{U} \sum_{u=1}^{U} r_{u,s}. \tag{28}$$

7. Compare T_{CFCPSC_s} with the decision threshold γ_{FC} in order to reach a decision on the occupation state of the s-th sub-band: decide $\mathcal{H}_0$ if $T_{\text{CFCPSC}_s} < \gamma_{\text{FC}}$ or $\mathcal{H}_1$ if $T_{\text{CFCPSC}_s} \geq \gamma_{\text{FC}}$.
8. Make the final decision as $\mathcal{H}_0$ when each decision in each sub-band is $\mathcal{H}_0$ or as $\mathcal{H}_1$ when at the minimum one sub-band decision is $\mathcal{H}_1$.

2.4.2. CFCPSC with DF

The CFCPSC with DF, denoted as CFCPSC-DF, deals with each antenna as a single receiver. In [11], it is shown that the alteration of the original CFCPSC, in this case, is similar to having L single-antenna receivers rather than a single L- antenna SU. Every one of the SUs divide the whole bandwidth into S sub-bands, makes an occupation decision in the sub-band level, combines these decisions, finds a local occupation decision regarding the presence or absence of a PU signal in the sensed band, and forwards this occupation decision to the fusion center in order to make a global collaborative decision. The steps 1, 2, 3, 4, and 5 of this altered CFCPSC-DF are the same as the first ones of the modified CFCPSC-SF in Section 2.4.1. The remaining steps are as follows:

6. Find the CFCPSC $T_{\text{CFCPSC}_{u,s}} = r_{u,s}$ statistic at each SU for the s-th sub-band.
7. Compare $T_{\text{CFCPSC}_{u,s}}$ with a local decision threshold γ_u in order to decide on the occupation state of the s-th sub-band: when $T_{\text{CFCPSC}_{u,s}}$ is greater than $\geq \gamma_u$, decides $\mathcal{H}_1$, otherwise decide $\mathcal{H}_0$.
8. At each SU, make a occupation decision as $\mathcal{H}_0$ if all local sub-band decisions are also $\mathcal{H}_0$ or as $\mathcal{H}_1$ if at least one local sub-band decision is $\mathcal{H}_1$ and then send this decision to the FC.
9. At the fusion center, combine the U decisions and make a global collaborative decision as $\mathcal{H}_0$ when all received decisions are $\mathcal{H}_0$ or as $\mathcal{H}_1$ otherwise.

3. Simulation Results and Discussions

We present some Monte Carlo simulation results of the GLRT-based and CFCPSC-based approaches in multiantenna-CR-based centralized CSS under the seldom adopted SS scenario of correlated received signals at the antenna arrays of SUs combined with uncalibrated antenna arrays of SUs. Results are for (i) GLRT-DF with the fusion rules AND (GLRT-DF-AND), OR (GLRT-DF-OR), and MAJ (GLRT-DF-MAJ), (ii) GLRT-SF, -WSF, -EF, and -WEF, and (iii) CFCPSC-SF and -DF. Calibration errors at each antenna branch follow the DN model proposed in (2) with $\sigma_{l,u}^2 = 1$.

Simulations consider one single-antenna PU transmitter, the number of SUs and antennas given by the pairs $(U, L) = \{(2,9), (3,6), (6,3), (9,2)\}$, and $N = 30$ samples at each SU antenna per sensing period, unless stated otherwise.

The PU signal was assumed to be a baseband BPSK signal with five independent and identically distributed samples per symbol with six symbols per sensing period. Each SU

has an average SNR according to Table 1. The PU signal powers at SUs are unequal and computed as $P_{l,u} = \sigma_{l,u}^2 \times 10^{\mathrm{SNR}_u/10} = 10^{\mathrm{SNR}_u/10}$ according to the corresponding desired average SNR in Table 1. Notice that the average SNR of the secondary network is always $(1/U)\sum_{u=1}^{U} \mathrm{SNR}_u = -10$ dB independently of the number of SUs, U, in Table 1, which is a challenging SS scenario for detecting PU signals.

Table 1. Average SNRs at each SU according to the number of SUs, U.

	SNR for the u-th SU, dB								
	$u=1$	$u=2$	$u=3$	$u=4$	$u=5$	$u=6$	$u=7$	$u=8$	$u=9$
$U=2$	-12	-8							
$U=3$	-12	-10	-8						
$U=6$	-12	-11.2	-10.4	-9.6	-8.8	-8			
$U=9$	-12	-11.5	-11	-10.5	-10	-9.5	-9	-8.5	-8

Each sensing channel has $Z = 6$ non-zero taps and mimics a slow-FS Rayleigh fading channel. Table 2 shows the adopted normalized power gains. Finally, the CFCPSC algorithm adopts $S = 5$ sub-bands for both SF and DF.

Table 2. Power delay profile of the channel between primary user and secondary user.

Path Index	**1**	**2**	**3**	**4**	**5**	**6**
Propagation delays in μs	0	3	8	11	13	21
Path gains in dB	0	-7	-15	-22	-24	-19

Figure 2 depicts the AUC values as a function of the correlation coefficient ρ for fixed $U = 2$ SUs, $L = 9$ antennas, $N = 30$ samples at every single SU antenna per sensing period, (a) $\xi = 0$, i.e., the antenna array of u-th SU is assumed to be calibrated by a suitable technique and (b) $\xi = 1$, when the level of noise power variation at the front-ends of multiantenna-based SUs is in the worst case in the adopted system model. If the DN is null, i.e., $\xi = 0$, the performance ranking of adopted detectors is: GLRT-SF, closely followed by GLRT-WSF, followed by, GLRT-WEF, GLRT-EF, CFCPSC-SF, GLRT-DF-MAJ, GLRT-DF-AND, GLRT-DF-OR, and CFCPSC-DF, for all range of ρ values. In this scenario, in general, the presence of correlation, i.e., for $\rho > 0$, leads to a poorer detection performances. However, notice that the CFCPSC-based approaches have a considerable improvement performance under the presence of DN, i.e., for $\xi = 1$. The opposite occurs for the GLRT-based approaches. We postpone the discussions regarding the DN variation.

Figures 3 and 4 present several numerical results according to the configurations established in the aforementioned paragraphs adopting AUC versus ξ. However, the correlation model uses the correlation coefficient as $\rho = 0$ or $\rho = 1$ to simulate a sensing scenario such that the received signal samples at each antenna array are uncorrelated or have maximum correlation, respectively. The adoption of these correlation coefficients yields the maximum and minimum benefit of the spatial diversity order of antenna arrays, which leads to the best and the worst cases in terms of detection performances of each detector from the perspective of correlated and uncorrelated received signals. Simulations aim at analyzing the influence of having calibration errors combined with signal correlation on the detection performances of GLRT-based approaches compared to CFCPSC-based ones. The pairs of graphs marked as (a), (b) and (c), (d) in Figure 3 show numerical results for $U = \{2,3\}$ and $L = \{9,6\}$, and under uncorrelated, $\rho = 0$, and correlated, $\rho = 1$, received signal samples at each antenna array, respectively. In a similar way, the pairs of graphs marked as (a), (b) and (c), (d) in Figure 4 show numerical results for $U = \{6,9\}$ and $L = \{3,2\}$.

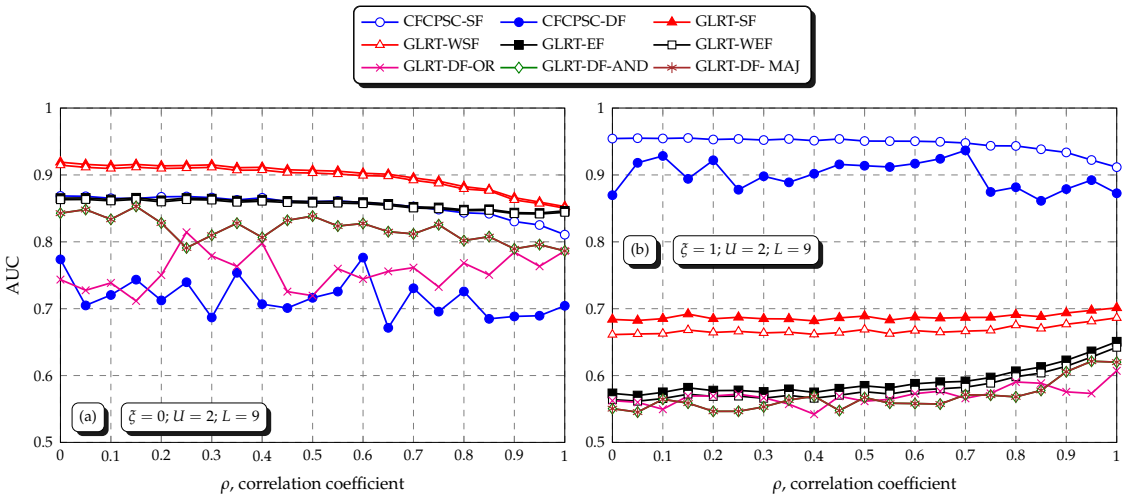

Figure 2. AUCs versus the correlation coefficient for $U = 2$ SUs and $L = 9$ antennas. (**a**) $\xi = 0$, absence of DN; (**b**) $\xi = 1$, presence of DN. This figure is better viewed in color.

First of all, it is worth emphasizing that the adoption of the DN model proposed in (2) led to considerably different results in terms of performance ranking compared to those corresponding results presented in [20] for uncorrelated received signals and unequal signal and noise powers (remembering that [20] considers $\rho = 0$, and $\xi = 0.8$ according to (2)). For example, choosing $U = 3$, $L = 6$, $\rho = 0$, and $\xi = 0.8$, the performance ranking of adopted detectors is, in [20]: GLRT-WSF followed by CFCPSC-SF, GLRT-WEF, GLRT-DF-OR, GLRT-EF, GLRT-SF, GLRT-DF-MAJ, and GLRT-DF-AND, while in Figure 3 the performance ranking is: CFCPSC-SF followed by CFCPSC-DF, GLRT-SF, GLRT-WSF, and GLRT-EF closely followed by GLRT-WEF and GLRT-DF-AND, -MAJ, and -OR. Besides, performance gaps between detectors adopted in [20] are also, in general, considerably larger than shown in Figure 3. Yet, performance rankings of Figures 3 and 4 are consistent with those presented in [23] for FS sensing channels and $\rho = 1$ for the majority of detectors (remembering that differently from this paper, [23] considers equal signal and noise powers among SUs and antennas per SU, i.e., it adopts the same average SNR at each SU and $\xi = 0$ according to (2), which justify some few differences compared to Figures 3 and 4).

The numerical analysis of Figures 3 and 4 unveils that the presence of DN at the antennas of SUs, which occurs when $\xi > 0$, may be highly detrimental to the detection performances of GLRT-based approaches, independently of the values of U, L, and ρ. See, for example, that the AUCs for any GLRT curve decrease as ξ increases. The poorer detection performances of the GLRT, in this case, are credited to the higher levels of calibration errors for larger values of ξ that directly impact the elements of the sample covariance matrices, their eigenvalues, and consequently, the resulting test statistic for distinguishing between noise only, $\mathcal{H}_0$, and noise plus PU signal, $\mathcal{H}_1$, in the sensed PU band. Surprisingly, the opposite occurs with the CFCPSC-based approaches. In this case, the presence of DN is interestingly beneficial to the detection performances of the CFCPSC since its AUCs, for any curve, increase as ξ increases, independently of the values of U, L, and ρ. These improvements in detection performances indicate that the benefits of having antennas with noise powers below the nominal noise power in a given sensing period, i.e., $\bar{\sigma}^2_{l,u} < \sigma^2_{l,u}$, outperform the penalties of having $\bar{\sigma}^2_{l,u} > \sigma^2_{l,u}$ in a given sensing period in the case of the CFCPSC, especially for large ξ. For a better understanding of the above statement, let us consider, for instance, a numerical example with $\xi = 0.8$. Notice that in this case, $\bar{\sigma}^2_{l,u} \in [(1-\xi)\sigma^2_{l,u}, (1+\xi)\sigma^2_{l,u}] = [0.2, 1.8]$, in which $\sigma^2_{l,u} = 1$. According to Figures 3 and 4, one can easily notice that the benefits of having $0.2 \leq \bar{\sigma}^2_{l,u} < 1$ in a given sensing instant, which results in an instantaneous SNR $P_{l,u}/\bar{\sigma}^2_{l,u}$ larger than the average SNR $P_{l,u}/\sigma^2_{l,u}$ of the received signal at the l-th antenna of u-th SU, i.e., $P_{l,u}/\bar{\sigma}^2_{l,u} > P_{l,u}/\sigma^2_{l,u}$, is larger than the penalties of having $1 < \bar{\sigma}^2_{l,u} \leq 1.8$ in a given sensing instant, which

results in an instantaneous SNR smaller than the average SNR of the received signal at the l-th antenna of u-th SU, i.e., $P_{l,u}/\bar{\sigma}^2_{l,u} < P_{l,u}/\sigma^2_{l,u}$. The aforementioned performance is in accordance with the results shown in Figure 2b when compared to Figure 2a.

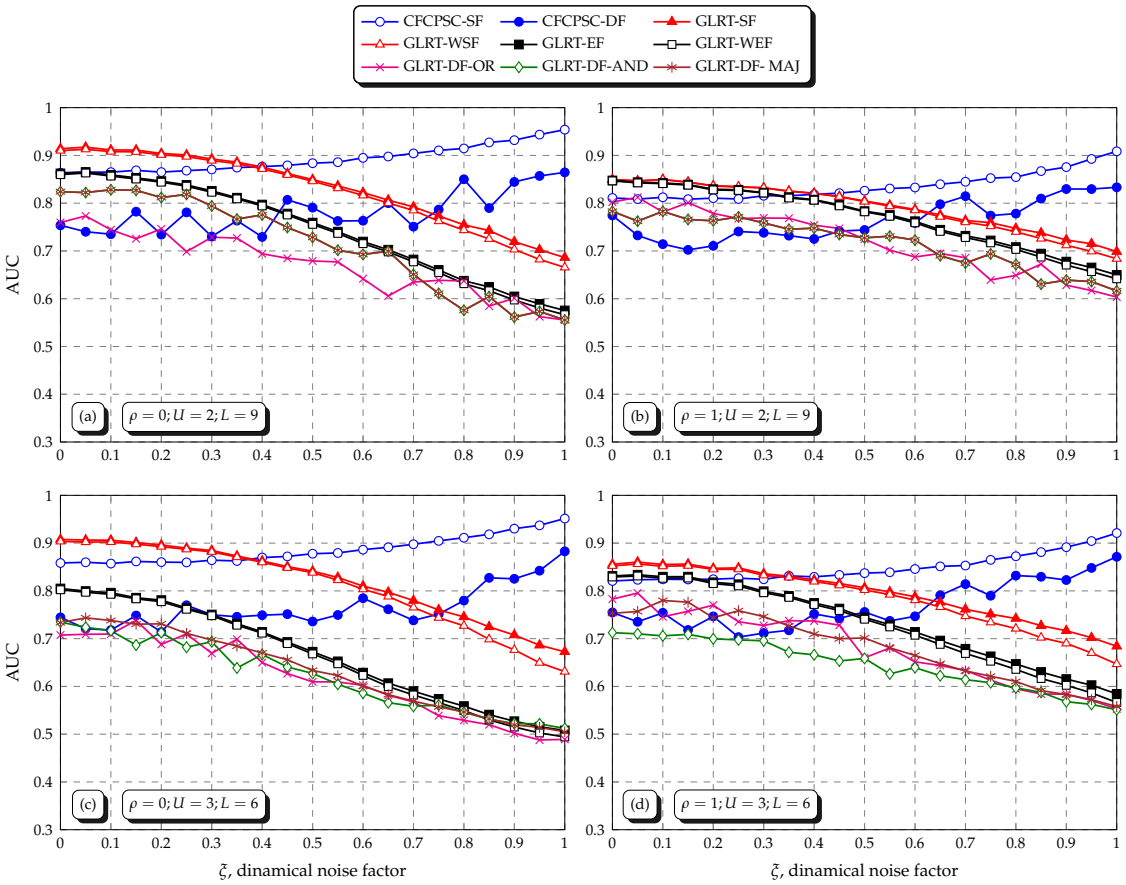

Figure 3. AUCs versus DN factor, ξ, for $U = 2$ SUs and $L = 9$ antennas (graphs (**a**,**b**)) and $U = 3$ SUs and $L = 6$ antennas (graphs (**c**,**d**)). This figure is better viewed in color.

Notice from Figures 3 and 4 that the GLRT-DF, -EF, and -WEF are more sensitive to the number of antennas per SU than the CFCPSC, since increasing or decreasing L may considerably increase or decrease the detection performances of the GLRT in these cases, especially for larger values of ξ and independently of ρ. Figure 4, for instance, depicts the worst cases where some detectors have the AUCs below or equal to 0.5, meaning that they are useless for larger values of ξ, independently of ρ. The increased or decreased detection performances of the GLRT-based approaches, in these cases, are consequences of the larger or smaller number of eigenvalues of the sample covariance matrices of SUs. In other words, increasing the number of eigenvalues of the sample covariance matrices increases the accuracy of GLRT statistics for distinguishing between $\mathcal{H}_0$ and $\mathcal{H}_1$. From these results, one can conclude that the GLRT-DF, -EF, and -WEF perform better when using smaller numbers of SUs with larger numbers of antennas per SU than larger numbers of SUs with smaller numbers of antennas per SU in the adopted SS scenarios. However, although the CFCPSC has, in general, more detection power than the GLRT; the GLRT-SF and -WSF perform better than CFCPSC for smaller values of ξ, independently of U, L, and ρ, which means that the GLRT-SF is a better choice in terms of detection performances for multiantenna-CR-based centralized CSS with calibrated antenna arrays in this case. The weighting schemes for WSF and WEF were effective in [20], but cannot bring any performance improvements here. On the contrary, results show that they are practically irrelevant in Figure 3 for $L = 9, 6$ and $0 \leq \xi \leq 1$ and may degrade or severely degrade the detection performances of the GLRT in Figure 4 with $L = 3, 2$ for larger values of ξ

compared to their corresponding unweighted versions, independently of ρ, respectively. Notice that smaller values of L reduce the accuracy in the computation of the weights, which represent the maximum likelihood estimate of noise power, or its square root, of each SU, and, consequently, the detection performances of the GLRT, especially for larger values of ξ. A comparison between graphs (a), (b) and (c), (d) for $\rho = 0$ and $\rho = 1$ in Figures 3 and 4 unveils that the GLRT and the CFCPSC suffer performance degradation with SF while GLRT-DF and -EF and CFCPSC-DF have performance improvements under correlated received signals for the majority of numerical results. Therefore, notice that the best-and-worst cases in terms of detection performances from the perspective of correlated and uncorrelated received signals depend on each detector since the existence of correlation benefits some test statistics while it penalizes others. The robustness to any values of U and L is a significant advantage of the CFCPSC-DF over GLRT-DF and -EF, which can be noticed particularly for large values of U and small values of L, independently of ρ. Finally, see from Figure 3a,b that the GLRT-DF-MAJ and GLRT-DF-AND rules have identical detection performances with 2 SUs since that the number of decisions $K = \lfloor U/2 + 1 \rfloor$ equals the number of SUs U.

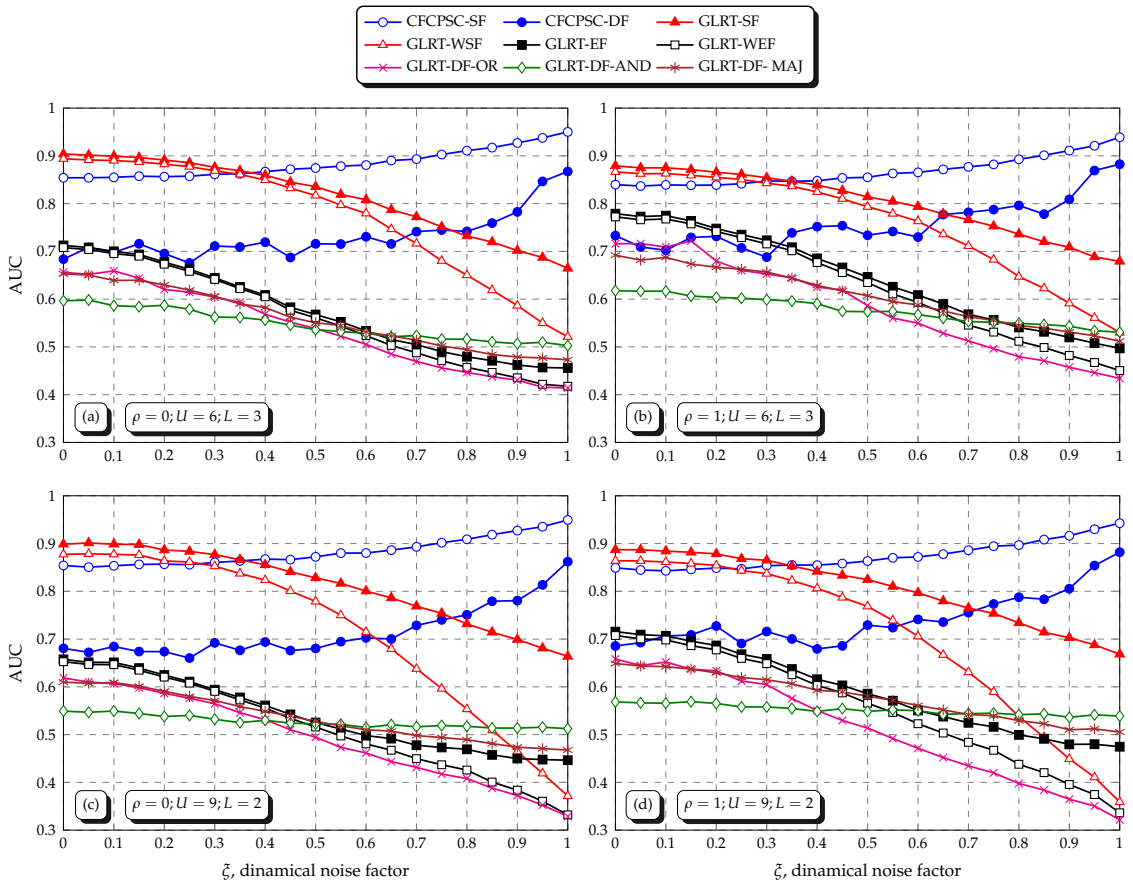

Figure 4. AUC versus DN factor, ξ, for $U = 6$ SUs and $L = 3$ antennas (graphs (**a**,**b**)) and $U = 9$ SUs and $L = 2$ antennas (graphs (**c**,**d**)). This figure is better viewed in color.

Now, in order to show a different scenario than $U \times L = 18$, as in the previous results, Table 3 shows some AUCs values for different combinations of U and L, under DN ($\xi = 0.8$) and correlation ($\rho = 0.8$). The same conclusions, as the ones obtained in Figures 3 and 4, can be found from the results of Table 3.

Table 3. AUCs for different values of U and L.

U	2			3			6			9		
L	3	6	9	3	6	9	3	6	9	3	6	9
CFCPSC-SF	0.729988	0.838198	0.895556	0.794639	0.89602	0.946796	0.901013	0.971991	0.990660	0.949289	0.99004	0.997944
CFCPSC-DF	0.651618	0.745349	0.765207	0.700577	0.77651	0.816878	0.760226	0.884537	0.880821	0.831518	0.887656	0.923810
GLRT-SF	0.545269	0.650442	0.749037	0.584686	0.741676	0.85266	0.737864	0.924277	0.983100	0.854241	0.983808	0.998689
GLRT-WSF	0.535668	0.637573	0.738003	0.552138	0.721738	0.842229	0.648853	0.907191	0.981202	0.749671	0.978559	0.998601
GLRT-EF	0.520655	0.584451	0.669108	0.508487	0.601918	0.694031	0.514222	0.639469	0.757595	0.520523	0.662543	0.800873
GLRT-WEF	0.513711	0.578112	0.662675	0.493975	0.589602	0.684807	0.486195	0.619507	0.744751	0.483049	0.637887	0.785588
GLRT-OR	0.508139	0.554845	0.600482	0.483197	0.555332	0.617140	0.46073	0.568586	0.626162	0.452316	0.575338	0.665070
GLRT-AND	0.523487	0.571553	0.649025	0.522549	0.577501	0.639655	0.533101	0.578388	0.644887	0.537838	0.573493	0.638000
GLRT-MAJ	0.523487	0.571553	0.649025	0.510522	0.578734	0.652747	0.523968	0.594999	0.692428	0.524387	0.608244	0.718336

4. Conclusions

This paper presented several performance analyses of blind statistical tests circular folding cooperative power spectral density split cancellation (CFCPSC) and generalized likelihood ratio test (GLRT) based on multiantenna cognitive radios in a centralized cooperative spectrum sensing under correlated received signals at the antennas of secondary users combined with unequal average primary user signal power and dynamical noise assuming uncalibrated antenna arrays and frequency-selective sensing channels. The analyses adopted the well-known eigenvalue-based GLRT with (i) sample fusion, weighted sample fusion, eigenvalue fusion, and weighted eigenvalue fusion, and (ii) decision fusion with the fusion rules AND, OR, and MAJ, and the recently proposed power spectral density-based CFCPSC with sample fusion and decision fusion. The spectrum sensing scenarios considered different numbers of secondary users and antennas per secondary user and aimed at investigating the influence of having calibration errors combined with signal correlations on the detection performances of the GLRT compared to the CFCPSC, which is known for being robust against dynamical noise powers. Results show that the GLRT is quite vulnerable to calibration errors with or without received signals correlations, while the CFCPSC improves its performances under calibration errors with or without received signals correlations, independently of the number of secondary users and antennas per secondary user. Besides, the weighting schemes used for the GLRT with weighted sample fusion and weighted eigenvalue fusion could not bring any benefits here and, on the contrary, caused severe performance degradation for higher levels of calibration errors. The GLRT with sample fusion and weighted sample fusion performed better than the CFCPSC with sample fusion only in lower levels of calibration errors. Correlations of received signals led to performance improvements for the GLRT with decision fusion and eigenvalue fusion/weighted eigenvalue fusion and the CFCPSC with decision fusion and performance degradation for the GLRT and CFCPSC with sample fusion. Robustness to the numbers of secondary users and antennas per secondary user is a relevant advantage of the CFCPSC with decision fusion over the GLRT with decision fusion and eigenvalue fusion. Results showed that the CFCPSC is the best choice for spectrum sensing under the adopted scenarios in the majority of the analyses.

Author Contributions: L.d.S.C. wrote the first versions of the manuscript, conceived the main ideas, and completed the majority of the work regarding the writing and review of the final manuscript. F.S.Q.Q.A. performed all simulations, with which L.d.S.C. assisted, and contributed to the preparation of the final version. R.A.A.d.S. revised all versions of the manuscript. All authors contributed equally in proofreading and technical discussions. All authors have read and agreed to the published version of the manuscript.

Funding: This work was partially supported by Fapemig (Grant No. APQ-00966-17), by São Paulo Research Foundation (Fapesp) (Grant No. 2021/06946-0), by CNPq (Grants No. 311470/2021-1 and 403827/2021-3), and by RNP, with resources from MCTIC (Grant No. 01245.010604/2020-14), under the 6G Mobile Communications Systems project of the Radiocommunication Reference Center (Centro de Referência em Radicomunicações-CRR) of the National Institute of Telecommunications (Instituto Nacional de Telecomunicações -Inatel), Brazil.

Conflicts of Interest: The authors declare no conflict of interest.

Abbreviations

The following abbreviations are used in this manuscript:

5G	Fifth generation
6G	Sixth generation
AGM	Arithmetic to geometric mean
AUC	Area under the curve
AWGN	Additive white Gaussian noise
BPSK	Binary phase-shift keying
CC	Control channel
CFCPSC	Circular folding cooperative power spectral density split cancellation
CPSC	Cooperative power spectral density split cancellation
CR	Cognitive radio
CSS	Cooperative spectrum sensing
DF	Decision fusion
DFT	Discrete Fourier transform
DN	Dynamical noise
ED	Energy detection
EF	Eigenvalue fusion
FC	Fusion center
FS	Frequency-selective
GLRT	Generalized likelihood ratio test
HD	Hard decision
IoT	Internet of things
MMED	Maximum-minimum eigenvalue detection
nCSS	Non-cooperative spectrum sensing
NU	Noise uncertainty
PSD	Power spectral density
PU	Primary user
QoE	Quality of experience
QoS	Quality of service
ROC	Receiver operating characteristic
SCM	Sample covariance matrix
SF	Sample fusion
SNR	Signal-to-noise ratio
SS	Spectrum sensing
SSE	Signal-subspace eigenvalue
SU	Secondary user
WEF	Weighted eigenvalue fusion
WRAN	Wireless regional area network
WSF	Weighted sample fusion

References

1. Chettri, L.; Bera, R. A Comprehensive Survey on Internet of Things (IoT) Toward 5G Wireless Systems. *IEEE Internet Things J.* **2020**, *7*, 16–32. [CrossRef]
2. Ghosh, A.; Maeder, A.; Baker, M.; Chandramouli, D. 5G Evolution: A View on 5G Cellular Technology Beyond 3GPP Release 15. *IEEE Access* **2019**, *7*, 127639–127651. [CrossRef]
3. Zhao, Y.; Yu, G.; Xu, H. 6G mobile communication networks: Vision, challenges, and key technologies. *Sci. Sin. Inform.* **2019**, *49*, 963–987. [CrossRef]
4. Brito, J.M.C.; Mendes, L.L.; Gontijo, J.G.S. Brazil 6G Project - An Approach to Build a National-wise Framework for 6G Networks. In Proceedings of the 2020 2nd 6G Wireless Summit (6G SUMMIT), Virtual, 17 March 2020; pp. 1–5. [CrossRef]
5. Akhtar, F.; Rehmani, M.H.; Reisslein, M. White space: Definitional perspectives and their role in exploiting spectrum opportunities. *Telecommun. Policy* **2016**, *40*, 319–331. [CrossRef]
6. Ivanov, A.; Tonchev, K.; Poulkov, V.; Manolova, A. Probabilistic Spectrum Sensing Based on Feature Detection for 6G Cognitive Radio: A Survey. *IEEE Access* **2021**, *9*, 116994–117026. [CrossRef]

7. Gao, R.; Li, Z.; Qi, P.; Li, H. A Robust Cooperative Spectrum Sensing Method in Cognitive Radio Networks. *IEEE Commun. Lett.* **2014**, *18*, 1987–1990. [CrossRef]
8. Patil, V.M.; Patil, S.R. A survey on spectrum sensing algorithms for cognitive radio. In Proceedings of the 2016 International Conference on Advances in Human Mach, Interaction (HMI), Kodigehalli, India, 3–5 March 2016; pp. 1–5. [CrossRef]
9. Wang, P.; Fang, J.; Han, N.; Li, H. Multiantenna-Assisted Spectrum Sensing for Cognitive Radio. *IEEE Trans. Veh. Technol.* **2010**, *59*, 1791–1800. [CrossRef]
10. Guimarães, D.A. Robust Test Statistic for Cooperative Spectrum Sensing Based on the Gerschgorin Circle Theorem. *IEEE Access* **2018**, *6*, 2445–2456. [CrossRef]
11. Bomfin, R.C.D.V.; de Souza, R.A.A.; Guimarães, D.A. Circular Folding Cooperative Power Spectral Density Split Cancellation Algorithm for Spectrum Sensing. *IEEE Commun. Lett.* **2017**, *21*, 250–253. [CrossRef]
12. Soni, B.; Patel, D.K.; Ding, Z.; Guan, Y.L.; Sun, S. On Sensing Performance of Multi-antenna Mobile Cognitive Radio conditioned on Primary User Activity Statistics. *IEEE Trans. Wireless Commun.* **2022**, *21*, 3381–3394. [CrossRef]
13. Zhang, R.; Lim, T.J.; Liang, Y.C.; Zeng, Y. Multi-antenna based spectrum sensing for cognitive radios: A GLRT approach. *IEEE Trans. Commun.* **2010**, *58*, 84–88. [CrossRef]
14. Taherpour, A.; Nasiri-Kenari, M.; Gazor, S. Multiple antenna spectrum sensing in cognitive radios. *IEEE Trans. Wirel. Commun.* **2010**, *9*, 814–823. [CrossRef]
15. López-Valcarce, R.; Vazquez-Vilar, G.; Sala, J. Multiantenna spectrum sensing for Cognitive Radio: Overcoming noise uncertainty. In Proceedings of the 2010 2nd Internatinal Workshop on Cognitive Information Processing, Elba Island, Italy, 14–16 June 2010. [CrossRef]
16. Ramirez, D.; Vazquez-Vilar, G.; Lopez-Valcarce, R.; Via, J.; Santamaria, I. Detection of Rank-*P* Signals in Cognitive Radio Networks with Uncalibrated Multiple Antennas. *IEEE Trans. Signal Process.* **2011**, *59*, 3764–3774. [CrossRef]
17. Taherpour, A.; Toghraei, M. A Universal Multiple Antenna Test for Spectrum Sensing. *IEEE Commun. Lett.* **2019**, *23*, 326–329. [CrossRef]
18. Sedighi, S.; Taherpour, A.; Sala, J. Spectrum Sensing Using Correlated Receiving Multiple Antennas in Cognitive Radios. *IEEE Trans. Wirel. Commun.* **2013**, *12*, 5754–5766. [CrossRef]
19. Pourgharehkhan, Z.; Taherpour, A.; Sala-Alvarez, J.; Khattab, T. Correlated Multiple Antennas Spectrum Sensing Under Calibration Uncertainty. *IEEE Trans. Wirel. Commun.* **2015**, *14*, 6777–6791. [CrossRef]
20. Costa, L.; Bomfin, R.; Guimarães, D.; de Souza, R. Performance of Blind Cooperative Spectrum Sensing under Nonuniform Signal and Noise Powers. *J. Commun. Inform. Syst.* **2018**, *33*, 158–171. [CrossRef]
21. *802.22-2011*; IEEE Standard for information technology–Local and Metropolitan Area Networks–SPECIFIC Requirements–Part 22: Cognitive Wireless RAN Medium Access Control (MAC) and Physical Layer (PHY) Specifications: Policies and Procedures for Operation in the TV Bands. IEEE: Piscataway, NJ, USA, 2011. [CrossRef]
22. Kim, H.; Kim, J.; Yang, S.; Hong, M.; Yoo, M.; Lee, W.; Shin, Y. An Effective MIMO-OFDM Transmission Scheme for IEEE 802.22 WRAN Systems. In Proceedings of the 2007 2nd International Conference on Cognitive Radio Oriented Wireless Networks and Communications, Orlando, FL, USA, 1–3 August 2007; pp. 394–399. [CrossRef]
23. Alves, F.S.Q.Q.; Costa., L.S.; de Souza, R.A.A. Multiantenna-Cognitive-Radio-Based Blind Spectrum Sensing Under Correlated Signals. In Proceedings of the 2021 IEEE Latin-American Conference on Communications (LATINCOM), Santo Domingo, Dominican Republic, 17–19 November 2021. [CrossRef]
24. Lee, I.G.; Son, J.B.; Lee, J.H.; Choi, E.Y.; Lee, S.K. Signal Receiving Apparatus and Method for Wireless Communication System Using Multiple Antennas. US Patent 8,811,537, 19 August 2014.
25. Krishnamoorthy, A.; Menon, D. Matrix inversion using Cholesky decomposition. In Proceedings of the 2013 Signal Processing: Algorithms, Architectures, Arrangements, and Applications (SPA), Poznan, Poland, 26–28 September 2013; pp. 70–72.
26. Villavicencio, M.A.G.; de Souza, R.A.A.; de Souza, G.C.; Yacoub, M.D. A Bivariate κ-μ Distribution. *IEEE Trans. Veh. Technol.* **2016**, *65*, 5737–5743. [CrossRef]
27. Wax, M.; Kailath, T. Detection of signals by information theoretic criteria. *IEEE Trans. Acoust. Speech Signal Process.* **1985**, *33*, 387–392. [CrossRef]